

# A Physics-Informed Neural Network approach for compartmental epidemiological models

C. Millevoi<sup>a,\*</sup>, D. Pasetto<sup>b</sup> and M. Ferronato<sup>a</sup>

<sup>a</sup>Department of Civil, Environmental and Architectural Engineering, University of Padova, via Marzolo 9, Padova, 35131 PD, Italy

<sup>b</sup>Department of Environmental Sciences, Informatics and Statistics, Ca' Foscari University of Venice, Via Torino, 155, Venezia Mestre, 30170 VE, Italy

---

## ARTICLE INFO

### Keywords:

Physics-Informed Neural Networks  
Epidemiological Models  
SIR Compartmental Model  
Nonlinear Inverse Problem  
Reproduction number

## ABSTRACT

Compartmental models provide simple and efficient tools to analyze the relevant transmission processes during an outbreak, to produce short-term forecasts or transmission scenarios, and to assess the impact of vaccination campaigns. However, their calibration is not straightforward, since many factors contribute to the rapid change of the transmission dynamics during an epidemic. For example, there might be changes in the individual awareness, the imposition of non-pharmacological interventions and the emergence of new variants. As a consequence, model parameters such as the transmission rate are doomed to change in time, making their assessment more challenging. Here, we propose to use Physics-Informed Neural Networks (PINNs) to track the temporal changes in the model parameters and provide an estimate of the model state variables. PINNs recently gained attention in many engineering applications thanks to their ability to consider both the information from data (typically uncertain) and the governing equations of the system. The ability of PINNs to identify unknown model parameters makes them particularly suitable to solve ill-posed inverse problems, such as those arising in the application of epidemiological models. Here, we develop a reduced-split approach for the implementation of PINNs to estimate the temporal changes in the state variables and transmission rate of an epidemic based on the SIR model equation and infectious data. The main idea is to split the training first on the epidemiological data, and then on the residual of the system equations. The proposed method is applied to five synthetic test cases and two real scenarios reproducing the first months of the COVID-19 Italian pandemic. Our results show that the split implementation of PINNs outperforms the standard approach in terms of accuracy (up to one order of magnitude) and computational times (speed up of 20%).

---

## 1. Introduction

Epidemiological models are nowadays fundamental to assist and guide policy makers in the fight against the spreading of diseases. This has been evident during the recent SARS-CoV-2 pandemic, when epidemiologists and scientists all over the world devoted their research to develop ad-hoc transmission models. Focusing, for example, on Italy, where the European outbreak started in February 2020, epidemiological models have been adopted to analyze different aspects of the epidemic: to determine the urgency to impose regional restrictions (Guzzetta et al., 2020); to analyze the impact of the national lockdown (Marziano et al., 2021b; Gatto et al., 2020); to explore the results of transmission scenarios after the release of the restrictions (Bertuzzo et al., 2020); to study the impact of the different variants and the vaccination campaign (Marziano et al., 2021a; Gozzi et al., 2022; Parolini et al., 2022); and to compute optimal strategies for the vaccine deployment in order to minimize the number of cases or deaths (Lemaitre et al., 2022; Ziarelli et al., 2023). Most of these studies describe the SARS-CoV-2 transmission using different variations of compartmental models. The basic SIR model is at the core of those more-complex epidemiological models. It subdivides the population of interest into compartments indicating the infectious status of each individual (i.e. susceptible, infected, or recovered individuals). The dynamic describes the mean contacts between susceptible and infected individuals, and thus, the average rate at which susceptible individuals transit to the infected compartment. The main model parameter is the rate of transmission of the infection,  $\beta$ . This is strictly related to the well known basic reproduction number,  $\mathcal{R}_0$ , representing the average number of secondary infections generated by one infected

---

\*Corresponding author

✉ [caterina.millevoi@phd.unipd.it](mailto:caterina.millevoi@phd.unipd.it) (C. Millevoi); [damiano.pasetto@unive.it](mailto:damiano.pasetto@unive.it) (D. Pasetto);  
[massimiliano.ferronato@unipd.it](mailto:massimiliano.ferronato@unipd.it) (M. Ferronato)  
ORCID(s): 0000-0001-6892-9826 (D. Pasetto)

individual in a totally susceptible population. The value of this quantity changes during an outbreak due to the temporal variations in human behavior (caused, for example, by changes in individual awareness or social distancing policies) and in the infectiousness of the virus. The effective reproduction number,  $\mathcal{R}_t$ , aims at describing the ongoing transmission in a changing system.

Data-driven methods provide effective estimates of  $\mathcal{R}_t$  based on the renewal equation (Cori et al., 2013; Pasetto et al., 2021; Trevisin et al., 2023), i.e., a convolution on the reported cases having as kernel the serial interval (the time interval between the symptom onset of an individual and its secondary infections). These data-driven estimates do not explicitly provide a relationship between the changes in  $\mathcal{R}_t$  and its possible causes, such as the implemented non pharmaceutical interventions or the vaccination campaigns. Compartmental models give a deeper understanding of the ongoing spreading of the disease and, at the same time, allow the computation of  $\mathcal{R}_t$  using the spectral radius of the next generation matrix (Mari et al., 2021; van den Driessche and Watmough, 2002; Diekmann et al., 1990). However, they require the assessment and calibration of time-dependent parameters.

Tracking the temporal variations in the model parameters is an essential but complex problem to follow and predict the spreading of a disease. Many studies tackle this problem using Bayesian inference, i.e., searching for the posterior distribution of the unknown parameters based on the available reported cases and the prior distribution. Among these approaches, we recall the iterative particle filter (Ionides et al., 2015), sequential data-assimilation schemes (Pasetto et al., 2017), or the use of subsequent Markov chain Monte Carlo (MCMC) (Parolini et al., 2022; Bertuzzo et al., 2020). Being based on random sampling, these approaches might result in low quality results and large computational times, due to the slow Monte Carlo convergence.

Here, we propose to adopt a deterministic approach based on Physics-Informed Neural Networks (PINNs). The idea behind PINNs is to exploit the universal approximation property of neural networks (Cybenko, 1989; Hornik et al., 1989) to estimate the solution of differential equation (Raissi et al., 2019). In practice, this is done by describing the state variables and, in case, the time-dependent parameters using Neural Networks (NNs). The parameters of the NNs are trained by seeking the minimum of a loss function based on both the misfit on the available data, and the residual of the differential equations governing the problem at hand, i.e., the SIR model equations in our case. Thus, the PINN functions fit the data and, at the same time, provide good approximations of the solutions of the differential equations.

The application of PINNs to epidemiological models became particularly relevant during the COVID-19 pandemic. Many studies used PINNs as an inverse-problem solvers, to calibrate the parameters of epidemiological compartmental models. However, the model parameters has frequently been considered constant in time, e.g. (Torku et al., 2021; Malinzi et al., 2022), or with particular periodic dependencies on time (Berkhahn and Ehrhardt, 2022). Schiassi et al. (2021) showed the computational efficacy of using PINNs to estimate constant parameters of different basic compartmental models under increasing levels of noise in the data. Long et al. (2021) considered a more realistic scenario, and used PINNs to accurately identify the time-varying transmission parameter in a SIRD model of COVID-19 when assimilating the reported infected cases in three USA States. Feng et al. (2022) proposed a similar approach to predict the number of active cases and removed cases in the US. Olumoyin et al. (2021) used PINNs to track the changes in transmission rate and the number of asymptomatic individuals for COVID-19, while Ning et al. (2023) presented a similar application to a SEIRD model during the first months of the Italian outbreak. Bertaglia et al. (2022) constrained PINNs to satisfy an asymptotic-preservation property to avoid poor results caused by the multiscale nature of the residual terms in the loss function. Building on top of these examples, our work aims to deeper explore the properties of PINNs as an inverse solver for the estimation of a time-dependent transmission rate in SIR models. In particular, we propose two modifications of the PINNs algorithm that grant faster convergence and more stable results.

The first proposed modification splits the PINN implementation in two steps. The motivation for this approach is that in the common PINN implementation for SIR-like models, the NNs representing the model state variables and, if present, the time-dependent parameters are calibrated together through the minimization of the loss function on the data and the model residual. This inverse problem is particularly complex and many epochs might be required to achieve convergence. Starting from the idea that the available epidemiological data, which are typically, the daily or weekly reported infections, is directly associated to a model state variable, the split PINN approach is based on the following two steps: as first, construct the NN of the state variable associated to the data, e.g., the infected compartment, by minimizing the loss function based on the data; as second, calibrate the other NNs for the remaining state variables and parameters based on the NN computed in the first step and the minimization of the residuals of the governing equations. We will refer to the traditional PINN approach as ‘joint approach’, in contrast to the described ‘split approach’.

The second proposed modification reduces the number of NNs considered in the PINN approximation and, consequently, simplifies the structure of the loss function. This simplification is possible because, in simple SIR-based

models, the transmission parameter and the infected compartment control the system dynamic. In fact, these functions allow to directly evaluate the other state variables, which are then redundant in the formulation of the loss function.

Our analysis compares the joint, split and reduced approaches in a sequence of synthetic test cases where we progressively challenge the structure of the transmission rate from constant, to a sinusoidal-like dependence on time, to a real scenario, and increase the noise on the synthetic reported data. The proposed test cases assume model parameters that are inspired by the first months of the COVID-19 outbreak in Italy. As a final example of application, the proposed PINN strategies are adapted in order to fit the real epidemiological data recorded in Italy. Due to the large uncertainties that characterize the real data on the reported infections, in this last setting we propose to include in the loss function also the data on the daily hospitalizations, which are a more reliable representation of the number of individuals with severe symptoms.

The paper is organized as follows. Section 2 presents the mathematical formulation of the proposed methods. It starts with the equations of the SIR model (Section 2.1), then it describes the joint and split implementations of PINNs (Section 2.2), and finishes with the modified schemes for the reduced approach (Section 2.3) and the extension to the hospitalized data (Section 2.4). The numerical results of the application of the proposed PINNs to seven test cases are illustrated in Section 3. Finally, Section 4 presents the discussion of the results and sums up the main conclusions.

## 2. Methods

### 2.1. The basic SIR model

The well-known SIR model is largely adopted for the theoretical analysis of epidemics, and lies at the core of several more complex epidemiological models for real applications. At a given time  $t$  [T], the individuals in a population of dimension  $N$  [-] are subdivided into compartments on the basis of their epidemiological status, in this case the susceptible ( $S$ ), the infected ( $I$ ), and the recovered ( $R$ ) individuals. The number of individuals in the three compartments changes in time under the assumption that, in a well mixed population, any susceptible individual can enter in contact with any infected individual, thus possibly becoming infected itself.

From a mathematical point of view, the strong form of the ordinary differential problem governing these dynamics can be stated as follows. Let  $\mathcal{T} = [t_0, t_f] \subseteq \mathbb{R}^+ \cup \{0\}$  be the time domain of interest, with  $t_0$  and  $t_f$  [T] the initial and final times of the simulation, respectively. Given the continuous functions  $\beta(t) : \mathcal{T} \rightarrow \mathbb{R}^+$  and  $\delta(t) : \mathcal{T} \rightarrow \mathbb{R}^+$ , find  $S(t) : \mathcal{T} \rightarrow [0, N]$ ,  $I(t) : \mathcal{T} \rightarrow [0, N]$ , and  $R(t) : \mathcal{T} \rightarrow [0, N]$  such that:

$$\begin{cases} \dot{S}(t) = -\frac{\beta}{N} I(t)S(t) \\ \dot{I}(t) = \frac{\beta}{N} I(t)S(t) - \delta I(t) \\ \dot{R}(t) = \delta I(t) \end{cases}, \quad \forall t \in \mathcal{T}, \quad (1)$$

and satisfying the initial conditions:

$$\begin{cases} S(t_0) = N - I_0 \\ I(t_0) = I_0 \\ R(t_0) = 0 \end{cases} \quad (2)$$

In Eqs. (1)-(2)  $\beta$  [T<sup>-1</sup>] is the transmission rate controlling the average rate of the infection,  $\delta$  [T<sup>-1</sup>] is the mean rate of removal of the infected individuals that become recovered, and  $I_0$  is the number of infected individuals (typically 1, but not necessarily) at the initial instant. Another relevant quantity used to set up the model is  $D = \delta^{-1}$ , i.e., the mean reproduction period [T] representing the average time spent by an individual in compartment  $I$ . Initial conditions for the spreading of a new disease assume that the population at the initial time is completely susceptible besides a small number  $I_0$  of infected individuals.

The basic reproduction number  $\mathcal{R}_0$  [-] associated to this model reads  $\mathcal{R}_0 = \beta(t_0)/\delta(t_0)$  and provides an estimate of the number of secondary infections generated by one infectious individual in a susceptible population, i.e. at the beginning of the epidemic. The threshold  $\mathcal{R}_0 > 1$  indicates the occurrence of an outbreak, while  $\mathcal{R}_0 < 1$  indicates that the number of infected individuals is rapidly decreasing. Note that, in a real population, the number of individuals in each compartment is a discrete variable, whose dynamic can be described by stochastic approaches, e.g., the Gillespie

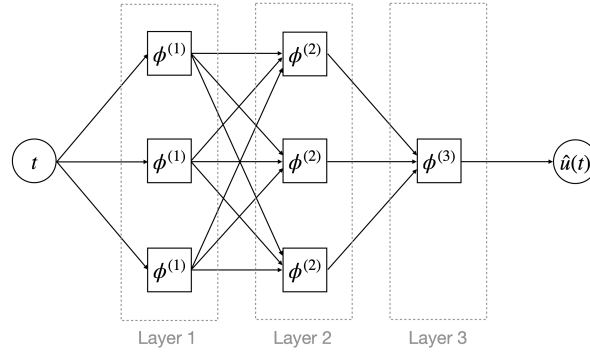


**Figure 1:** Sketch of a neural network with 2 hidden layers,  $n_0 = n_3 = 1$ , and  $n_1 = n_2 = 3$ .

method or discrete Markov chains. Hence, the continuous deterministic model in Equations (1)-(2) is a valuable representation of the mean process in large populations.

Standard numerical ODE solvers, such as Runge-Kutta-based methods, can provide an accurate solution to the differential problem (1)-(2). For  $\mathcal{R}_0 > 1$  and constant parameters, the solution depicts an initial exponential-like increase in the number of infections up to a peak, and then a fast decrease due to the depletion of susceptible individuals. However, it is clear that this dynamic does not correspond to what happens during an outbreak. The main challenge when using a model based on (1) to describe a real epidemic is that the transmission rate  $\beta$  and the mean reproduction period  $\delta^{-1}$  can change in time because of many factors: social behaviors (individual awareness, increase or decrease of gatherings, mobility, social distancing), non-pharmaceutical interventions (use of devices that reduce transmission - such as masks, introduction of lock-downs), changes in the pathogen infectiousness due to new variants, reduction of the susceptibility of the population due to vaccination campaigns. In this evolving scenario, the effective reproduction number  $\mathcal{R}_t$  [-] is the critical quantity that controls the spreading of the disease.  $\mathcal{R}_t$  is the equivalent of  $\mathcal{R}_0$  in time, i.e.,  $\mathcal{R}_t = \beta(t)/\delta(t) \cdot S(t)/N$ , taking into account that the number of susceptible individuals decreases and the main parameters controlling the spreading of the disease generally change. An essential element for a reliable simulation is therefore the assessment of  $\mathcal{R}_t$ , hence  $\beta(t)$  and  $\delta(t)$  along with the compartment  $S(t)$ , from the available epidemiological data. In the following we will assume that  $\delta$  is constant in time.

## 2.2. PINN solution to the SIR model

Here we develop and analyze a PINN-based approach to simultaneously solve the problem (1)-(2) and estimate the temporal values of the reproduction number by using a time series of infectious individuals as basic epidemiological information. A standard NN aims to reconstruct an unknown function  $u$  from the knowledge of some training data points. The NN approximating a generic  $u$ , denoted throughout this work by  $\hat{u}$ , is the recursive composition of the function:

$$\boldsymbol{\Sigma}^{(l)}(\mathbf{x}^{(l)}) = \boldsymbol{\phi}^{(l)}(\mathbf{W}^{(l)}\mathbf{x}^{(l)} + \mathbf{b}^{(l)}), \quad (3)$$

where  $\mathbf{W}^{(l)} \in \mathbb{R}^{n_l \times n_{l-1}}$ ,  $\mathbf{b}^{(l)} \in \mathbb{R}^{n_l}$ , and  $\boldsymbol{\phi}^{(l)}$  are weights, biases, and activation functions of the  $l$ -th layer, respectively. The last layer is the output layer, the others are the hidden layers. We denote with  $n_l$  the number of neurons in layer  $l$ . Activation functions are user-specified functions with limited range, which are generally non linear in order to provide a source of non linearity to the NN and maintain low weight values. The Matlab-inspired notation  $\boldsymbol{\phi}(\mathbf{x})$  means that the function  $\boldsymbol{\phi}$  is applied to each component of the vector  $\mathbf{x}$ . Let  $L$  be the number of hidden layers. If  $u : \mathcal{T} \rightarrow \mathbb{R}$  is the solution of an ordinary differential equation in the domain  $\mathcal{T}$ , the input of the first layer reads  $\mathbf{x}^{(1)} = t \in \mathcal{T}$ , so  $n_0 = 1$ , and the output of the last layer  $\hat{u}$  is a scalar, so  $n_{L+1} = 1$ . Then, the NN for  $u$  formally reads:

$$\hat{u}(t) = \boldsymbol{\Sigma}^{(L+1)} \circ \boldsymbol{\Sigma}^{(L)} \circ \dots \circ \boldsymbol{\Sigma}^{(1)}(t). \quad (4)$$

Figure 1 schematizes a neural network with 2 hidden layers. The NN depends on the set of weights and biases, which are trained through an optimization algorithm so as to minimize an appropriate loss function defined as the mean squared error of  $\hat{u}$  over the set of training points. In the case of PINNs, the information from the governing equations of the

physical system is introduced in a weak form in the loss function by adding the residual of the differential equations evaluated at some collocation points (Raissi et al. (2017a,b)).

For the SIR model (1)-(2), we assume that the training data points for the fitting are the reported infections. Let  $\tilde{I}_j$  be the number of reported infected individuals at times  $\tilde{t}_j$ ,  $j = 1, \dots, N_D$ . This might be subject to reporting errors, thus, in general  $\tilde{I}_j \neq I(\tilde{t}_j)$ . The residual of the governing equations is computed over  $N_C$  collocation points.

We aim at finding an approximate NN representation for the susceptible, infected and recovered individuals,  $\hat{S}(t)$ ,  $\hat{I}(t)$ ,  $\hat{R}(t)$ , respectively, along with the transmission rate  $\hat{\beta}(t)$ . Since the state variables  $S, I, R$  span an extremely wide range of values (from zero to the population size  $N > 10^6$ ), the functional search is optimized by a proper scaling:

$$S(t) = CS_s(t_s), \quad I(t) = CI_s(t_s), \quad R(t) = CR_s(t_s), \quad (5)$$

where  $C[-]$  is an appropriate constant and  $t_s$  is the dimensionless scaled temporal variable,  $t_s = (t - t_0)/(t_f - t_0)$ . The system of ODEs (1) for the scaled variables becomes:

$$\begin{cases} \dot{S}_s(t_s) = -C_1\beta_s(t_s)I_s(t_s)S_s(t_s) \\ \dot{I}_s(t_s) = C_1\beta_s(t_s)I_s(t_s)S_s(t_s) - C_2I_s(t_s) \\ \dot{R}_s(t_s) = C_2I_s(t_s) \end{cases}, \quad t_s \in [0, 1], \quad (6)$$

where  $\beta_s(t_s) : [0, 1] \rightarrow \mathbb{R}^+$ ,  $C_1 = (t_f - t_0)C/N$  and  $C_2 = (t_f - t_0)\delta C$ . The initial conditions (2) are correspondingly scaled as well as the infectious data  $\tilde{I}_j = C\tilde{I}_{s,j}$  at times  $\tilde{t}_{s,j} = (\tilde{t}_j - t_0)/(t_f - t_0)$ .

The SIR model (6) does not consider death and birth processes and assumes a negligible mortality rate of the disease. Thus, the total population  $N$  is constant in time and equal to  $N = S + I + R$ . Under these hypotheses, the PINN model needs only two NNs representing the behavior of the population: one for the state variable of the susceptible individuals  $\hat{S}_s$ , and one for the infected individuals  $\hat{I}_s$ . The number of recovered individuals is computed as  $\hat{R}_s = \frac{N}{C} - \hat{I}_s - \hat{S}_s$ . A third NN is included for the estimation of the transmission rate  $\hat{\beta}_s$ . This approach consistently reduces the number of parameters to be tuned during the training.

It is important to underline that the state variables represent the number of individuals in a compartment, thus they all have positive outputs. Training the model without imposing this condition could lead to nonphysical negative NNs outputs. The non-negative constraint can be imposed in the NN in two alternative ways: inserting a penalty term for the negative values of the NNs (weak constraint) or building the NN architecture so as to allow for positive values only (hard constraint). The latter prescription can be met by setting the output activation function, i.e., the one related the last layer,  $\phi^{(L+1)}$ , equal for example to the square function. An experimental comparison between the two approaches shows that the latter is generally more effective and provides more robust results. The numerical outcomes that follow are therefore obtained by using the hard constraint prescription for the non-negativity of the solution. The same constraint is adopted to entail a positive value for  $\beta_s$ .

The selection of the loss function is one of the most sensitive steps in the PINN approach, given the multi-objective nature of the method. Using the Mean Squared Error (MSE) as loss measure, the objective is to minimize the mismatch on the  $N_D$  data:

$$\mathcal{L}_D(\hat{I}_s) = \omega_D \frac{1}{N_D} \sum_{j=1}^{N_D} \left[ \hat{I}_s(\tilde{t}_{s,j}) - \tilde{I}_{s,j} \right]^2, \quad (7)$$

the squared norm of the residual of Equations (6) evaluated on  $N_C$  collocation points  $\{\tilde{t}_{s,i}\}_{i=1}^{N_C}$ :

$$\mathcal{L}_{ODE}(\hat{S}_s, \hat{I}_s, \hat{\beta}_s) = \frac{1}{N_C} \sum_{i=1}^{N_C} \omega_S \left[ \frac{d\hat{S}_s}{dt_s} + C_1\hat{\beta}_s\hat{I}_s\hat{S}_s \right]^2 \Big|_{\tilde{t}_{s,i}} + \omega_I \left[ \frac{d\hat{I}_s}{dt_s} - C_1\hat{\beta}_s\hat{I}_s\hat{S}_s + C_2\hat{I}_s \right]^2 \Big|_{\tilde{t}_{s,i}} + \omega_R \left[ \frac{d\hat{R}_s}{dt_s} - C_2\hat{I}_s \right]^2 \Big|_{\tilde{t}_{s,i}}, \quad (8)$$

and the misfit on the initial conditions:

$$\mathcal{L}_{IC}(\hat{S}_s, \hat{I}_s) = \omega_{S_0} \left[ \hat{S}_s(0) - \frac{N - I_0}{C} \right]^2 + \omega_{I_0} \left[ \hat{I}_s(0) - \frac{I_0}{C} \right]^2 + \omega_{R_0} \hat{R}_s^2(0), \quad (9)$$

where  $\omega_*$  are proper weights needed to balance the relative importance of the entries arising from each contribution to the global MSE value.

We explore two possible approaches for the construction of the PINN model, indicated as *joint* or *split*. The joint approach aims to simultaneously calibrate  $\hat{S}_s$ ,  $\hat{I}_s$  and  $\hat{\beta}_s$  by minimizing the joint loss function corresponding to the sum of  $\mathcal{L}_D$ ,  $\mathcal{L}_{ODE}$  and  $\mathcal{L}_{IC}$ :

$$\mathcal{L}_{\text{joint}}(\hat{S}_s, \hat{I}_s, \hat{\beta}_s) = \mathcal{L}_D(\hat{I}_s) + \mathcal{L}_{ODE}(\hat{S}_s, \hat{I}_s, \hat{\beta}_s) + \mathcal{L}_{IC}(\hat{S}_s, \hat{I}_s). \quad (10)$$

By distinction, the split approach subdivides the overall problem. First,  $\hat{I}_s$  is independently calibrated on the data error  $\mathcal{L}_D$  (7) only. In this case, a standard NN is used with weight  $\omega_D = 1$ , thus obtaining a differentiable regression function for the data. The only-data regression is followed by a fully-physics-informed regression, where the parameters defining  $\hat{S}_s$  and  $\hat{\beta}_s$  are trained by minimizing:

$$\mathcal{L}_{\text{split}}(\hat{S}_s, \hat{\beta}_s) = \mathcal{L}_{ODE}(\hat{S}_s, \hat{\beta}_s) + \mathcal{L}_{IC}(\hat{S}_s). \quad (11)$$

### 2.3. Reduced SIR model

The system of ODEs in (1) can be further reduced by directly considering the definition of the effective reproduction number  $\mathcal{R}_t$ . By easy developments, the model (1) becomes:

$$\begin{cases} \dot{I}(t) = \delta(\mathcal{R}_t - 1)I(t) \\ \dot{S}(t) = -\delta\mathcal{R}_t I(t) \end{cases}, \quad t \in [t_0, t_f]. \quad (12)$$

where the unknown functions are  $I(t)$  and  $S(t)$ , and the state variable  $R(t)$  is simply obtained from the consistency relationship  $R(t) = N - S(t) - I(t)$ . The initial conditions (2) still hold. The new system (12) can be solved sequentially by integrating the upper equation first and then computing  $S(t)$  from the second equation.

This approach reduces the number of functions that are approximated by NNs to two, i.e.,  $I$  and  $\mathcal{R}_t$ , and eliminates any redundant term in the loss function minimized in the PINN approach. The same scaling as in Equation (5) is used for the state variable  $I$ , so that the upper equation in (12) reads:

$$\dot{I}_s(t_s) = \delta(t_f - t_0)(\mathcal{R}_t - 1)I_s(t_s), \quad t_s \in [0, 1]. \quad (13)$$

The NNs approximating the variables of interest, i.e.,  $\hat{I}_s$  and  $\hat{\mathcal{R}}_t$ , can be obtained by minimizing the mismatch on data  $\mathcal{L}_D$  (eq. (7)) and the squared norm of the residual of Equation (13) on  $N_C$  collocation points:

$$\mathcal{L}_{r,ODE}(\hat{I}_s, \hat{\mathcal{R}}_t) = \frac{1}{N_C} \sum_{i=1}^{N_C} \left[ \frac{d\hat{I}_s}{dt_s} - \delta(t_f - t_0)(\hat{\mathcal{R}}_t - 1)\hat{I}_s \right]^2 \Big|_{\bar{t}_{s,i}} \quad (14)$$

Notice that in this case the contributions in  $\mathcal{L}_D$  and  $\mathcal{L}_{r,ODE}$  have a consistent size, hence there is no need for introducing the weight parameters  $\omega_*$  to balance the loss function terms. For this reason, we simply set  $\omega_D = 1$  in the expression (7).

The joint and split approaches can be formulated for this PINN-based model as well. The joint approach consists in training simultaneously the NNs  $\hat{I}_s$  and  $\hat{\mathcal{R}}_t$  by minimizing the total loss function:

$$\mathcal{L}_{r,\text{joint}}(\hat{I}_s, \hat{\mathcal{R}}_t) = \mathcal{L}_D(\hat{I}_s) + \mathcal{L}_{r,ODE}(\hat{I}_s, \hat{\mathcal{R}}_t). \quad (15)$$

By distinction, the split approach implies training  $\hat{I}_s$  on the data only by the minimization of  $\mathcal{L}_D$  in Equation (7). Then, the time-dependent parameter  $\hat{\mathcal{R}}_t$  is obtained by minimizing:

$$\mathcal{L}_{r,\text{split}}(\hat{\mathcal{R}}_t) = \mathcal{L}_{r,ODE}(\hat{\mathcal{R}}_t). \quad (16)$$

Notice that in the reduced PINN model no initial condition is set, but we let the model deduce it from the data. From a theoretical viewpoint, initial conditions are not necessary because  $\hat{I}_s$  is obtained from the data, while the governing differential equation (13) is used to calibrate  $\hat{\mathcal{R}}_t$ . This outcome is relevant because it replicates what typically happens in a real-case scenario, where there is no actual knowledge about the instant of beginning of the epidemic outbreak. In fact, the case 0 in most outbreaks is unknown and the conventional start of the epidemic has a number of infected individuals that is usually largely underestimated. The use of the reduced modeling approach makes it possible to remove the term related to the initial condition from the loss function.

## 2.4. SIR model with the hospitalization compartment

The reported infections can be often affected by large uncertainties. Especially at the beginning of an epidemic outbreak, the disease cannot be easily recognized, either because of the difficulty of correctly identifying the symptoms, or the absence of well-established detection and surveillance procedures, or the impossibility of reaching and testing all the people infected by the disease. Moreover, these data can be strongly affected by territorial peculiarities and the logistic of testing facilities. Hence, founding an epidemiological model on these pieces of information can undermine its reliability. A much less uncertain epidemiological datum is the daily number of individuals that require to be hospitalized. This is fraction of the overall number of infected individuals, however such a value can be representative of the entire  $I$  compartment by assuming that hospitalization is needed over a certain common threshold level of symptoms in the population.

We introduce a new variable,  $H$ , defined as:

$$H(t) = \delta\sigma I(t), \quad (17)$$

where  $\sigma$  represents the fraction of infected individuals moving to the hospitalized compartment. Note that also parameter  $\sigma$  might change in time, for example because of the insurgence of more aggressive variants or the improvement of home treatment. A more convenient formulation uses the cumulative number  $\Sigma_H$  of hospitalized individuals:

$$\Sigma_H(t) = \int_{t_0}^t H(z) dz. \quad (18)$$

The new formulation of the updated SIR model can be therefore stated as follows. Given  $\mathcal{R}_t : \mathcal{T} \rightarrow \mathbb{R}^+$ ,  $\sigma(t) : \mathcal{T} \rightarrow [0, 1]$ , and  $\delta(t) : \mathcal{T} \rightarrow \mathbb{R}^+$ , find  $\Sigma_H(t) : \mathcal{T} \rightarrow [0, N]$ ,  $I(t) : \mathcal{T} \rightarrow [0, N]$ , and  $S(t) : \mathcal{T} \rightarrow [0, N]$  such that:

$$\begin{cases} \dot{\Sigma}_H(t) = \delta\sigma I(t) \\ \dot{I}(t) = \delta(\mathcal{R}_t - 1)I(t) \\ \dot{S}(t) = -\mathcal{R}_t\delta I(t) \end{cases}, \quad \forall t \in \mathcal{T}, \quad (19)$$

with  $R(t) = N - I(t) - S(t)$ , the initial conditions (2) and  $\Sigma_H(t_0) = 0$ . The available information from the actual epidemiological data is the daily variation  $\Delta_H$  of the cumulative number of hospitalized individuals:

$$\Delta_H(t) = \Sigma_H(t) - \Sigma_H(t-1) \simeq \dot{\Sigma}_H(t), \quad (20)$$

whose values represents the training dataset for the PINN approximation of system (19). As previously done, the functional search of the approximating NNs is carried out on the properly scaled quantities  $I(t) = CI_s(t_s)$  (see Eq. (5)) and:

$$\Delta_H(t) = C_H \Delta_{H,s}(t_s), \quad (21)$$

with  $C_H$  the scaling factor. The upper equation in system (19) with the scaled quantities reads:

$$C_H \Delta_{H,s}(t_s) = \delta C \sigma_s(t_s) I_s(t_s), \quad (22)$$

with  $\sigma_s : \mathcal{T} \rightarrow [0, 1]$ , while the second scaled equation is the same as in (13). Hence, the NNs needed to solve the SIR model with hospitalization data are  $\hat{\Delta}_{H,s}$ ,  $\hat{I}_s$ ,  $\hat{\sigma}_s$ , and  $\hat{\mathcal{R}}_t$ . The training data points for the fitting are both the scaled reported infections  $\tilde{I}_{s,j}$  and the hospitalizations  $\tilde{\Delta}_{H,s,j}$  at the scaled times  $\tilde{t}_{s,j}$ ,  $j = 1, \dots, N_D$ . The NNs can be obtained by minimizing the mismatch (7) on the infection data and on the hospitalization data:

$$\mathcal{L}_H = \frac{1}{N_D} \sum_{j=1}^{N_D} \left[ \hat{\Delta}_{H,s}(\tilde{t}_{s,j}) - \tilde{\Delta}_{H,s,j} \right]^2, \quad (23)$$

and the squared norm of the residuals of Eqs. (13) and (22) on  $N_C$  collocation points:

$$\mathcal{L}_{H,ODE}(\hat{\Delta}_{H,s}, \hat{I}_s, \hat{\sigma}_s, \hat{\mathcal{R}}_t) = \frac{1}{N_C} \sum_{i=1}^{N_C} \left[ \frac{d\hat{I}_s}{dt_s} - \delta(t_f - t_0)(\hat{\mathcal{R}}_t - 1)\hat{I}_s \right] \Big|_{\tilde{t}_{s,i}}^2 + \frac{1}{N_C} \sum_{i=1}^{N_C} \left[ \hat{\Delta}_{H,s} - \frac{\delta C \hat{\sigma}_s}{C_H} \hat{I}_s \right] \Big|_{\tilde{t}_{s,i}}^2. \quad (24)$$

The joint approach consists in the simultaneous estimate of  $\hat{\Delta}_{H,s}$ ,  $\hat{I}_s$ ,  $\hat{\sigma}_s$ , and  $\hat{\mathcal{R}}_t$  by finding the minimum to the functional:

$$\mathcal{L}_{H,\text{joint}}(\hat{\Delta}_{H,s}, \hat{I}_s, \hat{\sigma}_s, \hat{\mathcal{R}}_t) = \mathcal{L}_D(\hat{I}_s) + \mathcal{L}_H(\hat{\Delta}_{H,s}) + \mathcal{L}_{H,ODE}(\hat{\Delta}_{H,s}, \hat{I}_s, \hat{\sigma}_s, \hat{\mathcal{R}}_t). \quad (25)$$

As for the PINN solution to the reduced SIR model, it is not necessary to include the mismatch on the initial conditions into the global loss function (25) because they are met through the available training data. Moreover, also the use of non-unitary weights  $\omega_*$  for the different contributions to  $\mathcal{L}_{H,\text{joint}}$  is not required since all terms are likely to have a similar magnitude.

In the split approach,  $\hat{\Delta}_{H,s}$  is directly trained with the hospitalization data only by minimizing  $\mathcal{L}_H$  in Equation (23). Then,  $\hat{I}_s$  is computed from (22) as:

$$\hat{I}_s = \frac{C_H}{\delta C} \frac{\hat{\Delta}_{H,s}}{\hat{\sigma}_s}, \quad (26)$$

and  $\hat{\sigma}_s$  and  $\hat{\mathcal{R}}_t$  are trained by minimizing:

$$\mathcal{L}_{H,\text{split}}(\hat{\sigma}_s, \hat{\mathcal{R}}_t) = \frac{1}{N_D} \sum_{j=1}^{N_D} \left[ \frac{C_H}{\delta C} \frac{\hat{\Delta}_{H,s}(\tilde{t}_{s,j})}{\hat{\sigma}_s(\tilde{t}_{s,j})} - \tilde{I}_{s,j} \right]^2 + \frac{1}{N_C} \sum_{i=1}^{N_C} \left\{ \frac{C_H}{C} \left[ \frac{d}{dt_s} \left( \frac{\hat{\Delta}_{H,s}}{\delta \hat{\sigma}_s} \right) - (t_f - t_0)(\hat{\mathcal{R}}_t - 1) \frac{\hat{\Delta}_{H,s}}{\hat{\sigma}_s} \right] \right\}^2 \Big|_{\tilde{t}_{s,i}}. \quad (27)$$

In real-world scenarios, the new daily infections is a more common piece of information than the total number of infected individuals. In order to include these data in the PINN model, we introduce the cumulative number  $\Sigma_I$  of infected individuals:

$$\Sigma_I(t) = \int_{t_0}^t I(z) dz. \quad (28)$$

The variation of  $\Sigma_I$  in time coincides with negative variation of the class of susceptible individuals  $S(t)$ , so we can simply update the SIR model with hospitalization data (19) by replacing the last equation with:

$$\dot{\Sigma}_I(t) = \delta \mathcal{R}_t I(t) \quad (29)$$

Since the available information is the daily variation  $\Delta_I$  of the cumulative number of infected individuals:

$$\Delta_I(t) = \Sigma_I(t) - \Sigma_I(t-1) \simeq \dot{\Sigma}_I(t), \quad (30)$$

we use these values as training data set. As usual, scaled values are considered such as  $\Delta_I = C \Delta_{I,s}$  and we assume that the set of scaled values  $\tilde{\Delta}_{I,s,j}$  is available at the training scaled times  $\tilde{t}_{s,j}$ ,  $j = 1, \dots, N_D$ , instead of  $\tilde{I}_{s,j}$ . The mismatch of  $\hat{\Delta}_{I,s}$ , i.e., the NN approximating  $\Delta_{I,s}$ , with the data is measured by:

$$\mathcal{L}_I = \frac{1}{N_D} \sum_{j=1}^{N_D} \left[ \hat{\Delta}_{I,s}(\tilde{t}_{s,j}) - \tilde{\Delta}_{I,s,j} \right]^2, \quad (31)$$

while the squared norm of the residual reads:

$$\begin{aligned} \mathcal{L}_{HI,ODE}(\hat{\Delta}_{H,s}, \hat{\Delta}_{I,s}, \hat{I}_s, \hat{\sigma}_s, \hat{\mathcal{R}}_t) &= \frac{1}{N_C} \sum_{i=1}^{N_C} \left[ \frac{d\hat{I}_s}{dt_s} - \delta(t_f - t_0)(\hat{\mathcal{R}}_t - 1)\hat{I}_s \right]^2 \Big|_{\tilde{t}_{s,i}} + \frac{1}{N_C} \sum_{i=1}^{N_C} \left[ \hat{\Delta}_{H,s} - \frac{\delta C \hat{\sigma}_s}{C_H} \hat{I}_s \right]^2 \Big|_{\tilde{t}_{s,i}} + \\ &\quad \frac{1}{N_C} \sum_{i=1}^{N_C} \left[ \hat{\Delta}_{I,s} - \delta \hat{\mathcal{R}}_t \hat{I}_s \right]^2 \Big|_{\tilde{t}_{s,i}}. \end{aligned} \quad (32)$$

Hence, with the joint approach we aim at minimizing the functional:

$$\mathcal{L}_{HI,\text{joint}}(\hat{\Delta}_{H,s}, \hat{\Delta}_{I,s}, \hat{I}_s, \hat{\sigma}_s, \hat{\mathcal{R}}_t) = \mathcal{L}_I(\hat{\Delta}_{I,s}) + \mathcal{L}_H(\hat{\Delta}_{H,s}) + \mathcal{L}_{HI,ODE}(\hat{\Delta}_{H,s}, \hat{\Delta}_{I,s}, \hat{I}_s, \hat{\sigma}_s, \hat{\mathcal{R}}_t). \quad (33)$$



	State variables	Estimated parameters	Reference values	Training data
Case 1	$S, I, R$	$\beta$ (constant)	$\beta_0 = 0.6 \text{ d}^{-1}$	$\tilde{I}_j$ (Poisson error)
Case 2	$S, I, R$	$\beta$ (time-dependent)	Synthetic $\beta$	$\tilde{I}_j$ (Poisson error)
Case 3	$S, I, R$	$\beta$ (time-dependent)	COVID-19 $\mathcal{R}_t$	$\tilde{I}_j$ (Poisson error)
Case 4	$I$	$\mathcal{R}_t$	Synthetic $\beta$	$\tilde{I}_j$ (40% Gaussian error)
Case 5	$I, \Delta_H$	$\mathcal{R}_t, \sigma$ (time-dependent)	Synthetic $\beta, \sigma$	$\tilde{I}_j$ (40% Gaussian error), $\tilde{\Delta}_{H,j}$ (Poisson error)
Case 6	$\Delta_I, \Delta_H$	$\mathcal{R}_t, \sigma$ (constant)	COVID-19 $\mathcal{R}_t$	$\tilde{\Delta}_{I,j}, \tilde{\Delta}_{H,j}$ (COVID-19 dataset)
Case 7	$\Delta_I, \Delta_H$	$\mathcal{R}_t, \sigma$ (time-dependent)	COVID-19 $\mathcal{R}_t$	$\tilde{\Delta}_{I,j}, \tilde{\Delta}_{H,j}$ (COVID-19 dataset)

**Table 1**

Different scenarios adopted to analyze the performance of the proposed PINN-based approaches.

By distinction, with the split approach we first train  $\hat{\Delta}_{H,s}$  by the available data (see Eq. (23)). Then, we use Equation (26) for  $\hat{I}_s$  and:

$$\hat{\Delta}_{I,s} = \frac{C_H}{C} \frac{\hat{\mathcal{R}}_t \hat{\Delta}_{H,s}}{\hat{\sigma}_s} \quad (34)$$

for  $\hat{\Delta}_{I,s}$ , and minimize the functional:

$$\mathcal{L}_{HI, \text{split}}(\hat{\sigma}_s, \hat{\mathcal{R}}_t) = \frac{1}{N_D} \sum_{j=1}^{N_D} \left[ \frac{C_H}{C} \frac{\hat{\mathcal{R}}_t \hat{\Delta}_{H,s}(\tilde{t}_{s,j})}{\hat{\sigma}_s(\tilde{t}_{s,j})} - \tilde{\Delta}_{I,s,j} \right]^2 + \frac{1}{N_C} \sum_{i=1}^{N_C} \left\{ \frac{C_H}{C} \left[ \frac{d}{dt_s} \left( \frac{\hat{\Delta}_{H,s}}{\hat{\sigma}_s} \right) - (t_f - t_0)(\hat{\mathcal{R}}_t - 1) \frac{\hat{\Delta}_{H,s}}{\hat{\sigma}_s} \right] \right\}^2 \Big|_{\tilde{t}_{s,i}}. \quad (35)$$

This choice for the split approach is based on the fact that hospitalization data are usually more reliable than infected individuals, hence they are more appropriate for an only-data regression training.

### 3. Numerical results

Our PINN-based approach is implemented by making use of the SciANN software library (Haghighat and Juanes, 2021), a Keras and TensorFlow wrapper specifically developed for physics-informed deep learning. We analyze the performance of the PINN-based approaches to estimate the state variables and identify the governing parameters of an epidemiological model mimicking the setup of the first 90 days of a COVID-like disease outbreak in Italy. The total population is set to  $N = 56 \times 10^6$  and the mean infectious period to  $D = 5$  days, which is an estimate used for COVID-19 (Bertuzzo et al., 2020). The initial value of infectious individuals  $I_0$  is set to 1. The accuracy of the trained NNs is evaluated by the 2-norm of the error with respect to the 2-norm of the reference solution:

$$e_r = \frac{\|\hat{y} - y_{ref}\|_2}{\|y_{ref}\|_2}, \quad (36)$$

where  $y$  can be either one of the state variables, or a time-dependent parameter. The relative error (36) is numerically computed by using 90 points equally spaced in the domain. We consider a number of scenarios, summarized in Table 1, differing for the reference SIR model and state variables of interest, the selection of the estimated governing parameters, and the available training data.

For the estimation of the transmission rate  $\beta(t)$  in the basic SIR model (1)-(2), we consider three different scenarios:

- Case 1: constant  $\beta$ . We use this scenario to compare the efficiency of the joint and split approaches (10) and (11), respectively;
- Case 2: synthetic time-dependent  $\beta(t)$ , where the reference values are provided as an analytical function;
- Case 3: an application to a real-case scenario where the reference  $\beta(t)$  is obtained from the estimates of  $\mathcal{R}_t$  in the first months of the COVID-19 epidemic outbreak in Italy.

In each case, the training data are the number of infectious individuals per day. These are synthetically generated by numerically integrating the system (1) using the selected reference function for  $\beta(t)$ . In particular, we used  $N_D = 90$  training data points (one value per day). To take into account possible reporting errors, the data  $\tilde{I}_j$  for each time  $\tilde{t}_j$  are obtained by sampling from a Poisson distribution having as mean  $I(\tilde{t}_j)$ . This kind of Poisson error is frequently assumed on data arising from a counting process. The infectious data and the epidemiological model are scaled by a factor  $C = 10^5$  (see eq. (5)). The NNs for  $\hat{S}_s$  and  $\hat{I}_s$  are built with 4 hidden layers, 50 neurons for each and tanh as activation function, while  $\hat{\beta}_s$  has 4 hidden layers with 100 neurons. In Case 1 the constant transmission rate is treated as a single parameter in the training. The output activation is set to  $x^2$ , as stated in Section 2.2. We consider  $N_C = 6000$  collocation points randomly sampled in  $[t_0, t_f]$  from a uniform distribution, Adam optimization algorithm (Kingma and Ba, 2017) with a learning rate equal to 0.001, and Glorot initialization (Glorot and Bengio, 2010) of the NNs. In the joint approach we trained the NNs for 5000 epochs with batches containing 100 training points, while in the split approach we set the number of epochs to 3000 for the data fitting training and to 1000 for the fully-physics-informed regression, with a batch size equal to 10 and 100, respectively. When the total number of training points ( $N_D + N_C$ ) is large, it is a good practice to use a mini-batch gradient descent as optimization algorithm, which splits the training dataset into small batches that are used to calculate model error and update model coefficients. The weights  $\omega_*$  are calibrated in the fitting process using the eigenvalues of the Neural Tangent Kernel (NTK) (Wang et al., 2021).

The reduced SIR model (12) is used to explore a more realistic scenario with strongly perturbed data. The motivation is that the data collected during the beginning of an outbreak are particularly subject to reporting errors. For example, the lack of a proper surveillance system and the low capacity in testing the presence of an infection may lead to an underestimation of the ongoing transmission. The joint and split approaches (15) and (16), respectively, are used to estimate the governing parameter  $\mathcal{R}_t$  in the following inverse problem:

- Case 4: synthetic time-dependent  $\beta(t)$  (as in Case 2), subject to a larger error noise on the infectious data.

The same NN architectures as described before for  $\hat{\beta}_s$  is used for  $\hat{\mathcal{R}}_t$  as well.

Finally, the performances of the joint and split PINN approaches in the SIR model with hospitalization data for the simultaneous calibration of parameters  $\sigma$  and  $\mathcal{R}_t$  are compared in the following realistic case scenarios:

- Case 5: an adaptation of the synthetic scenario described in Case 4, considering both infections data, hospitalization data, and a time-dependent  $\sigma$ ;
- Case 6: an application to the real data collected in Italy during the first months of the COVID-19 pandemic, considering as unknowns the value of  $\mathcal{R}_t$  (time-dependent) and  $\sigma$  (constant).
- Case 7: the same of Case 6, but having both  $\mathcal{R}_t$  and  $\sigma$  as functions of time.

The NN for  $\hat{\mathcal{R}}_t$  has 4 hidden layers with 100 neurons each,  $\hat{\sigma}_s$  has 10 hidden layers with 5 neurons each. In Case 5, the synthetic data of the daily hospitalizations,  $\{\tilde{\Delta}_{H,j}\}_{j=1}^{N_D}$ , are obtained by sampling from a Poisson distribution having as mean value the reference solution. The scaled values are obtained by setting  $C_H = 10^3$ . In Cases 6 and 7, we consider the epidemiological data provided by the Italian surveillance system EpiCentro (2020) from February 21<sup>st</sup>, 2020 to May 20<sup>th</sup>, 2020. The period coincides with the advent of the disease and its initial spread. The vaccination campaign was not started yet and possible reinfections are negligible. The Italian dataset contains the number of new daily hospitalizations and reported infections,  $\{\tilde{\Delta}_{H,j}\}_{j=1}^{N_D}$  and  $\{\tilde{\Delta}_{I,j}\}_{j=1}^{N_D}$ , respectively, and supplies an estimate of the COVID-19 reproduction number  $\mathcal{R}_t$  based on Cori et al. (2013). The scaled values are obtained by setting  $C$  and  $C_H$  equal to the maximum experimented values for  $\Delta_I$  and  $\Delta_H$ , respectively, in the 90 days taken into consideration. New infections are multiplied by a reporting ratio  $\alpha_r = 6$ , following the estimate from Italian Institute of Statistic based on the serological data (ISTAT, 2020).

### 3.1. Case 1: constant parameter

The first scenario assumes a constant transmission rate during the simulation. The reference value for the parameter is fixed to  $\beta = \beta_0 = 0.6 \text{ d}^{-1}$ , corresponding to a basic reproduction number  $\mathcal{R}_0 = 3$ , which is an estimate of the basic reproduction number in the COVID-19 epidemic in Italy. The resulting system dynamic is shown in Figure 2a. The evaluation of a constant parameter does not require an additional NN for  $\beta$ , and it is implemented through an object of the SciANN parameter class with the additional non-negative constraint. Both the joint and split approaches obtain solutions that match well the reference dynamic (see Figure 2a for the results of the split approach). Figure 2b shows

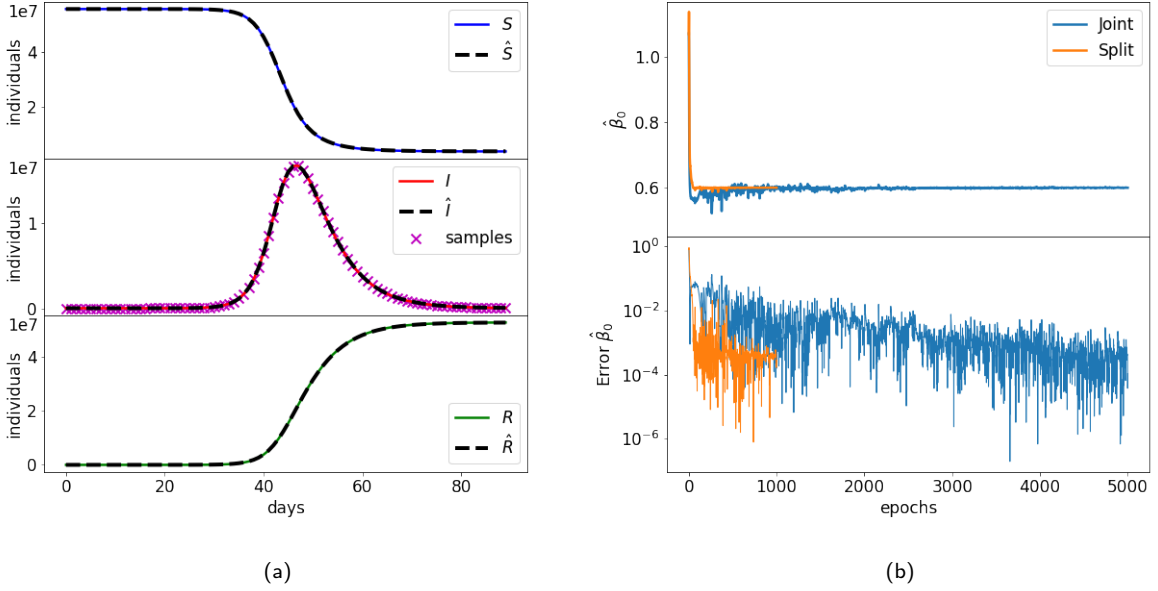


**Figure 2:** Case 1: Comparison between (a) reference solutions of the SIR model (1) and PINN approximations in the split approach; (b)  $\beta_0$  identification during training of the joint and the split methods.

	Daily data		Weekly data	
	Joint	Split	Joint	Split
Training time [s]	2223	719	1977	493
Error $S$	$2.763 \times 10^{-3}$	$6.221 \times 10^{-4}$	$2.833 \times 10^{-2}$	$2.247 \times 10^{-2}$
Error $I$	$3.846 \times 10^{-3}$	$8.444 \times 10^{-4}$	$4.544 \times 10^{-2}$	$4.245 \times 10^{-2}$
Error $R$	$3.258 \times 10^{-3}$	$7.434 \times 10^{-4}$	$3.276 \times 10^{-2}$	$2.491 \times 10^{-2}$
Error $\beta$	$5.086 \times 10^{-3}$	$3.587 \times 10^{-4}$	$4.693 \times 10^{-2}$	$5.187 \times 10^{-2}$
PINN $\hat{\beta}$	0.59738	0.60007	0.57323	0.56888

**Table 2**

Case 1: Training time, approximation errors, and estimations of the joint and split methods for a constant transmission rate  $\beta = 0.6d^{-1}$ . The daily and weekly infection data two correspond to  $N_D = 90$  and  $N_D = 13$ , respectively.

that the convergence of the joint approach to the reference  $\beta$  value is slower than the split approach. In fact, there are strong oscillations during training. The split approach mitigates these oscillations and reaches a faster convergence to the reference value.

Table 2 provides a quantitative comparison of the resulting errors for each state variable along with the training times. Note that for the split approach the sum of the only-data and physics-informed training is reported. In both approaches the PINN solution reaches an acceptable accuracy, with a relative error on the order of  $10^{-3}$  for all state variables, resulting in a good  $S$  estimate of the unknown parameter  $\beta$  as well. The split approach reduces the total training time about by a factor 3, and improves the accuracy with respect to the joint approach by one order of magnitude on average, hence it appears to be in this case largely preferable.

A second test is carried out by changing the amount of available data for the training. For instance, we consider only weekly values for the infection data, which are more likely to compensate the errors and oscillations of daily data. This reduces the number of training points to  $N_D = 13$ . The model is built and trained as stated in Section 3, with the difference that the training of  $\hat{I}_s$  in the split method is performed at each epoch on the whole data set and the mini-batches are not needed. Moreover, given the overall small size of the training data set, we can decrease the maximum number of epochs in the data regression from 3000 to 1000. Training times and approximation errors

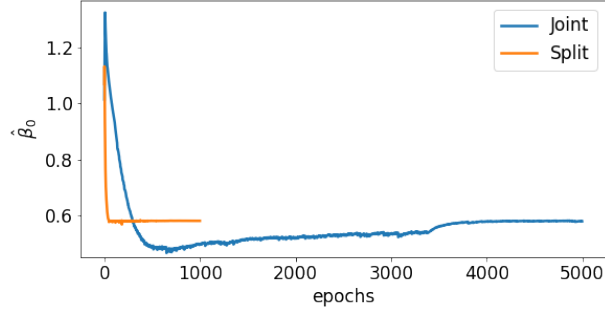


**Figure 3:** Case 1. Comparison between  $\beta_0$  identification during the training of the joint and split methods for the weekly infection data ( $N_D = 13$ ).

	Joint	Split
<b>Case 2</b>		
Training time [s]	1936	717
Error $S$	$1.814 \times 10^{-3}$	$3.381 \times 10^{-4}$
Error $I$	$2.501 \times 10^{-2}$	$7.754 \times 10^{-3}$
Error $R$	$2.288 \times 10^{-1}$	$4.251 \times 10^{-2}$
Error $\beta$	$2.678 \times 10^{-1}$	$4.127 \times 10^{-1}$
Error $\beta$ (last 70d)	$5.979 \times 10^{-2}$	$1.563 \times 10^{-2}$
<b>Case 3</b>		
Training time [s]	1906	726
Error $S$	$1.935 \times 10^{-3}$	$5.031 \times 10^{-4}$
Error $I$	$4.729 \times 10^{-3}$	$6.006 \times 10^{-3}$
Error $R$	$2.805 \times 10^{-2}$	$7.101 \times 10^{-3}$
Error $\mathcal{R}_t$	$4.692 \times 10^{-1}$	$6.988 \times 10^{-1}$
Error $\mathcal{R}_t$ (last 70d)	$5.341 \times 10^{-2}$	$6.701 \times 10^{-2}$

**Table 3**

Cases 2-3: Training time and approximation errors for the state variables and the estimated parameters with the joint and split approach.

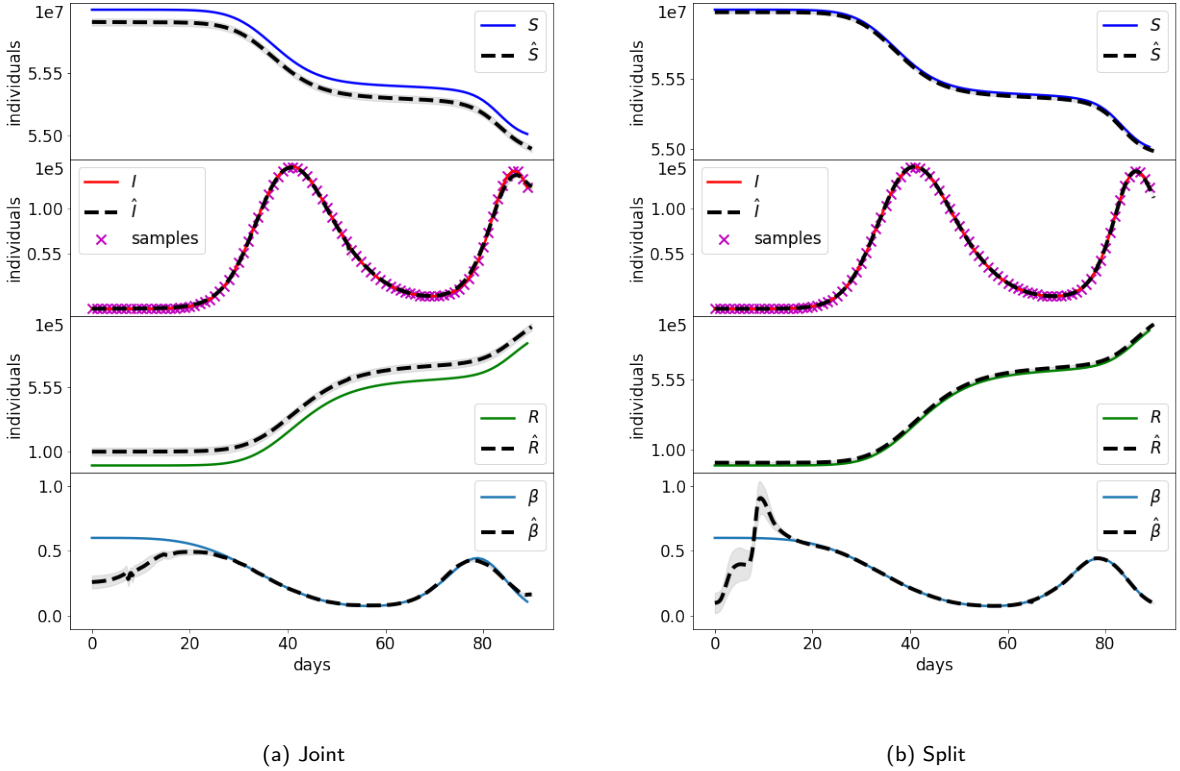
reported in Table 2 show an equivalent outcome in terms of accuracy, but with a strong gain in training time for the split approach. By reducing the number of samples the amount of information is smaller, hence the accuracy decreases with respect to a daily updated information. The convergence of the parameter  $\beta$  has a similar behavior to the one shown previously (Figure 3), with the split method reducing both the oscillations and the convergence time.

### 3.2. Cases 2 and 3: Time-dependent transmission rate $\beta(t)$

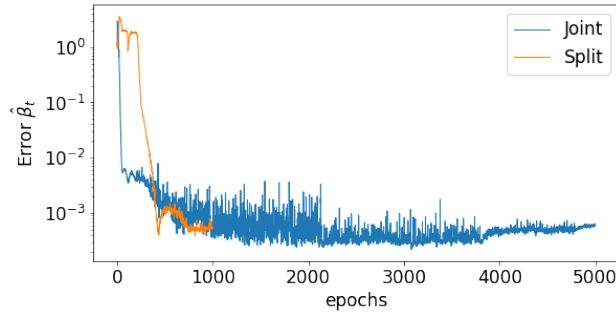
Case 2 consists of a simulation of disease spread according to the time-dependent transmission rate plotted in Figure 4. This  $\beta(t)$  behavior implies two waves of infection, with a maximum number of infectious individuals two orders of magnitude lower than in Case 1. As in Case 1, the numerical integration of the SIR model (1)-(2) provides the reference solution, from which we take the perturbed synthetic samples on the infectious individuals to train the neural networks. The transmission rate is here approximated by a NN,  $\hat{\beta}_s$ , since it is a function of time. Notice that even  $\hat{\beta}_s$  has a quadratic output activation to ensure its non-negativity.

Figure 4 shows the reference values of the unknowns and the corresponding NN approximations. The dotted lines correspond to the mean outcome from 10 different runs, while grey bands provide the confidence interval for one standard deviation. Usually, the split method provides more stable and accurate results, with smaller variations from one run to another. The higher stability and speed of convergence of the split approach can be also appreciated from the error behavior on  $\hat{\beta}_s$  during the training (Figure 5). The overall performance of the PINN approaches is summarized in Table 3.

Both approaches, however, fail to estimate the initial values of  $\beta$  (Figure 4). The low number of infected individuals and the presence of perturbed data produce an initial dynamic that the NNs erroneously learn by considering a larger



**Figure 4:** Case 2: Comparison between the reference solution of the SIR model and the PINN approximations with the joint (a) and split (b) approach. Grey bands provide the confidence interval for one standard deviation.



**Figure 5:** Case 2: Comparison between the errors on  $\hat{\beta}_s(t)$  during the training with the joint and split approach.

number of initial infected individuals and a lower initial transmission rate. These kinds of errors represent a common hurdle in epidemiology, as the evolution of a disease is extremely difficult to be identified at the beginning of the epidemic outbreak under the assumption of a temporal-depending transmission rate. For this reason, Table 3 provides also the error for  $\beta$  during the last 70 days of simulation. These small errors confirm the accuracy of the PINN estimates when the data provide a clear signal.

Case 3 has the same setting as Case 2 but considers as reference values for the effective reproduction number, and consequently the transmission rate in the model, the estimates supplied by the Italian health institute “Istituto

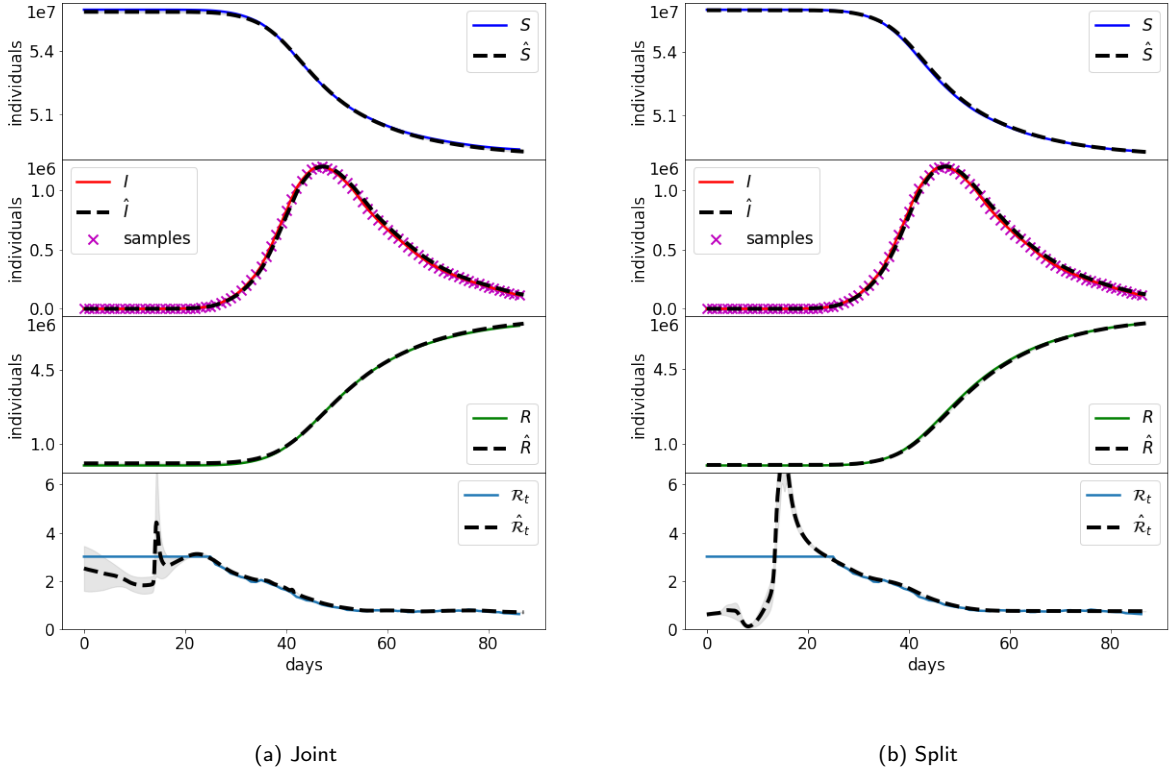


**Figure 6:** Case 3: Comparison between the reference solution of the SIR model and the PINN approximations with the joint (a) and split (b) approach. Grey bands provide the confidence interval for one standard deviation.

Superiore della Sanità” (ISS) (EpiCentro, 2020), depicted in Figure 6. For the first 20 days, the values have been kept equal to 3.012, in order to simulate the free transmission of the pathogen in a completely susceptible population without restrictions in contacts. This application to a realistic scenario reproduces the first three months of the Italian COVID-19 epidemic, from February 21 to May 20, 2020. The epidemiological data for training the PINN approaches are synthetically generated as in Case 2. Figure 6 and Table 3 contain the outcome of the joint and split methods. Similarly to Case 2, the estimation of the temporal evolution of the transmission rate is hard for the initial times. Both methods can achieve a good accuracy after the first 20 days, as it can be deduced from Figure 6 and from the errors associated to the last 70 days of the simulation. The matching is quite accurate, with relative errors on the order of  $10^{-3}$ , and the variance from 10 different runs is also limited. While the gain in accuracy of the split method is not so clear in this case, the benefit in the training duration is still relevant. Similar results in terms of accuracy has been obtained on these test cases when using the reduced implementation (12) of the split and joint approaches.

### 3.3. Cases 4 and 5: Reduced model and hospitalization data

Case 4 is used to investigate the performance of the joint and split approaches for the reduced model (12) in a synthetic scenario where the data are subject to large errors. The unknown time-dependent transmission rate is the same as the one of Case 2, whose corresponding reproduction number is shown in Figure 7.

The time domain is extended to  $t_f = 120$  days, which implies two complete waves of infection. To simulate the typically large uncertainties on the reported daily infections, we generate synthetic noisy data by perturbing the numerical solution for  $I(\tilde{t}_j)$  with a Gaussian error having zero mean and coefficient of variation of 40%. The data are then rounded to the closest integer with the negative values set to 0. Finally, the scaling factor  $C$  is set to  $10^5$  with  $N_D = 120$ .

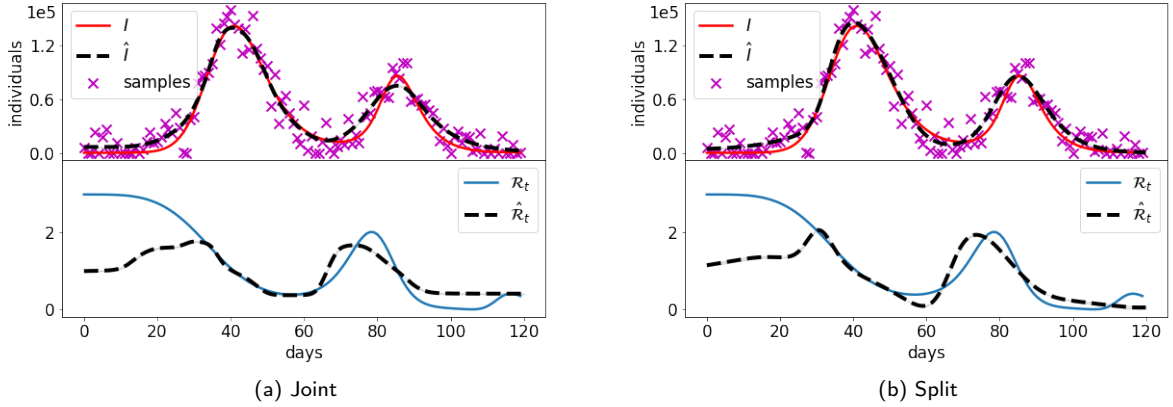


**Figure 7:** Case 4: Reference solution and PINN approximation with the joint (a) and split (b) approach in the reduced SIR model (12) and noisy data.

	Joint	Split
<b>Case 4</b>		
Training time [s]	1658	1053
Error $I$	$1.411 \times 10^{-1}$	$1.331 \times 10^{-1}$
Error $\mathcal{R}_t$	$4.961 \times 10^{-1}$	$4.744 \times 10^{-1}$
Error $\mathcal{R}_t$ (last 100d)	$3.141 \times 10^{-1}$	$3.336 \times 10^{-1}$
<b>Case 5</b>		
Training time [s]	1829	1445
Error $\Delta_H$	$8.783 \times 10^{-3}$	$4.722 \times 10^{-3}$
Error $I$	$1.209 \times 10^{-1}$	$7.434 \times 10^{-2}$
Error $\mathcal{R}_t$	$4.407 \times 10^{-1}$	$4.992 \times 10^{-1}$
Error $\mathcal{R}_t$ (last 100d)	$2.410 \times 10^{-1}$	$1.240 \times 10^{-1}$
Error $\sigma$	$3.858 \times 10^{-1}$	$1.417 \times 10^{-1}$
Error $\sigma$ (last 100d)	$2.626 \times 10^{-1}$	$1.145 \times 10^{-1}$

**Table 4**

Cases 4-5: Training time and approximation errors for the state variables and the estimated parameters with the joint and split approach.

The outcome of the PINN approximations are provided in Figure 7 and Table 4. The larger errors on the data reduce the accuracy in the estimate of the reproduction number. The two approaches are almost equivalent in terms of accuracy, but the split one has faster training times. Clearly, a large uncertainty in the training data reduces the reliability of the split approach, which mostly relies on this piece of information, while the joint approach compensates possible errors on data with the residuals of the governing equations. Nevertheless, the accuracy in the reproduction of the  $\mathcal{R}_t$  appears to be in any case fairly satisfactory, given the large reported errors.

In Case 5 we try to improve the  $\mathcal{R}_t$  estimates obtained in Case 4 by introducing the information on the daily hospitalizations. This entails that PINN trains also the NN for parameter  $\sigma$ , that describes the fraction of infected individuals that become hospitalized. The reference  $\sigma$  for this case is shown in Figure 8. The results of the joint and split approaches are summarized in Figure 8 and Table 4. The inclusion of more reliable data implies a better estimate of  $\mathcal{R}_t$  with respect to Case 4. This is particularly evident for the split approach, which is able to provide good estimates of both temporal depending parameters ( $\mathcal{R}_t$  and  $\sigma$ ), and thus, lower errors (Table 4).

### 3.4. Cases 6 and 7: Application to real data

Cases 6 and 7 use the same setup as Case 5, but with the real epidemiological data collected during the Italian COVID-19 epidemic outbreak. The fraction of the number of infected individuals that becomes hospitalized,  $\sigma$ , is

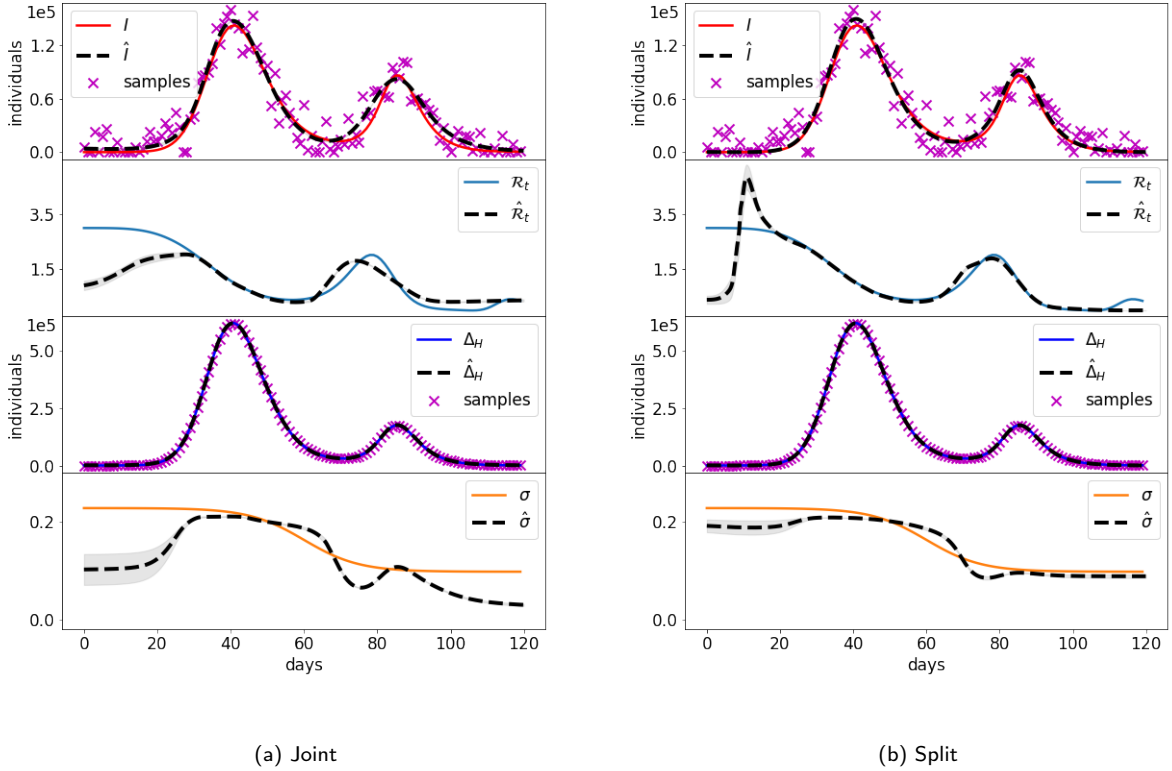


**Figure 8:** Case 5: Reference solution and PINN approximation in the joint (a) and split (b) approaches when considering the daily data on both hospitalizations and infections.

assumed to be constant in time in Case 6 and time-dependent in Case 7. The goal is to estimate  $\mathcal{R}_t$  and  $\sigma$  by means of the presented PINN approaches. We use the reproduction number evaluated by ISS (Figure 9) as a reference value for the comparison.

The results of the joint and the split approaches are shown in Figures 9 and 10 for Cases 6 and 7, respectively. In Case 6 the joint approach provides an acceptable accuracy on the new infection data, while the peak of the daily hospitalizations is underestimated (Figure 9a). The split approach, instead, is firstly trained on the daily hospitalization well retrieving these high-fidelity data. The second part of the training, considering both the daily infections and the reduced model equations, does not achieve the same level of accuracy for the infection data with respect to the joint approach (Figure 9b). For what concerns the estimation of  $\mathcal{R}_t$ , the joint approach strongly underestimates its value at the beginning of the epidemic. By distinction, the split approach provides a trend of  $\mathcal{R}_t$  that is fully consistent with the ISS estimates, i.e., a decrease during the first weeks of the epidemic, followed by an almost stationary value around 1 during the recession phase. The overall performance of the PINN approaches are summarized in Table 5.

Finally, considering a time-dependent  $\sigma$  (Case 7) helped both approaches to improve the estimate of both hospitalized and infectious data. Both approaches depict a similar trend for  $\sigma$ , showing that the fraction of infected individuals that became hospitalized decreased during March 2020 from a peak of about 23% to about 3%, which is a realistic outcome in the framework of Italian COVID-19 outbreak. The main differences among the two approaches are still at the beginning of the outbreak, where the joint approach suggests a lower value of  $\sigma$ , while underestimating the values of  $\mathcal{R}_t$ . The training time required by the split approach was about 40% of the of time for the joint approach (Table 5).



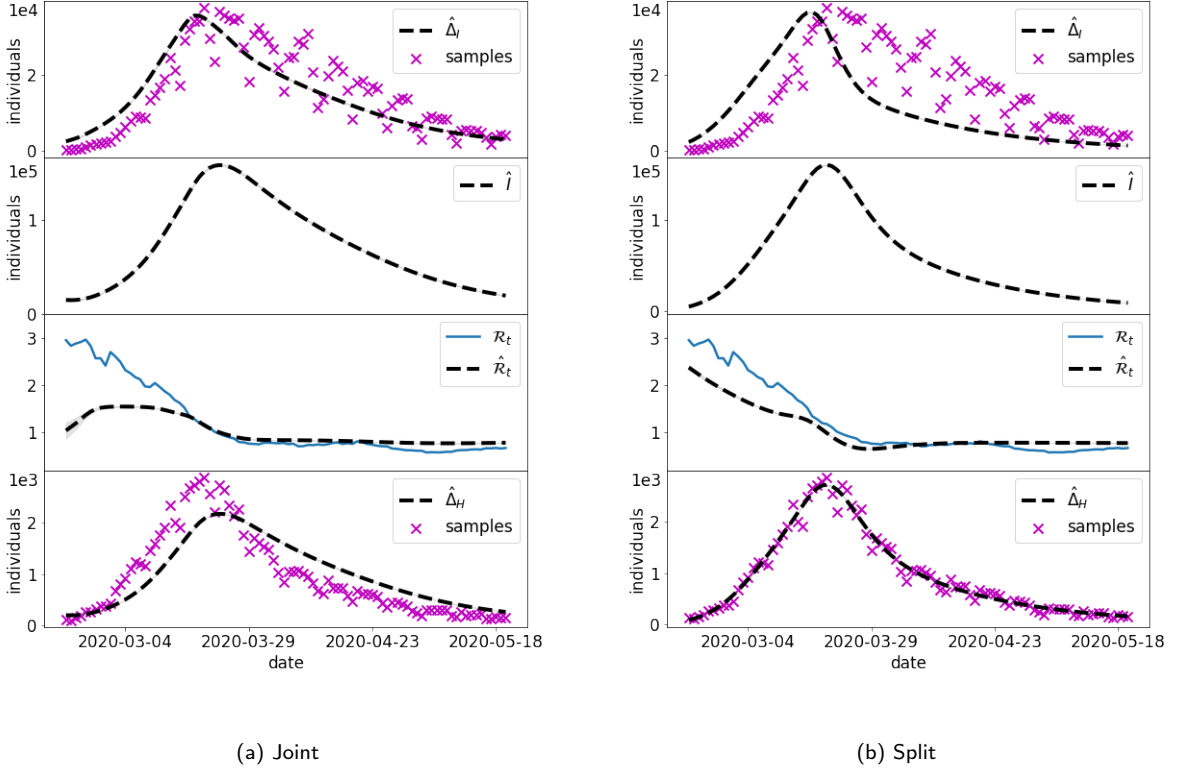


**Figure 9:** Case 6: PINN approximations with the joint (a) and split (b) methods for the real Italian COVID-19 outbreak with  $\sigma$  as a constant parameter. The blue trajectory of  $\mathcal{R}_t$  is the official estimate by ISS.

	Joint	Split
<b>Case 6</b>		
Training time [s]	1655	1042
Error $\mathcal{R}_t$	$3.881 \times 10^{-1}$	$2.495 \times 10^{-1}$
Error $\mathcal{R}_t$ (last 100d)	$1.474 \times 10^{-1}$	$1.821 \times 10^{-1}$
Estimated $\hat{\sigma}$	0.0686	0.0849
<b>Case 7</b>		
Training time [s]	1778	1101
Error $\mathcal{R}_t$	$3.646 \times 10^{-1}$	$2.236 \times 10^{-1}$
Error $\mathcal{R}_t$ (last 100d)	$1.682 \times 10^{-1}$	$1.742 \times 10^{-1}$

**Table 5**

Cases 6-7: Training time and approximation errors for the state variables and the estimated parameters with the joint and split approach.

#### 4. Discussion and conclusions

This work proposes two innovative ideas to improve the application of PINNs for the solution of SIR-based epidemiological models, and to estimate the time-dependent transmission rate, or the effective reproduction number, of an epidemic. The first idea consists in splitting the training of the NNs in two steps: the first step provides the fit on the epidemiological data, while the second step minimizes the residual on the model equations. The performance of the split approach has been compared to a standard PINN application, which trains simultaneously the NNs on

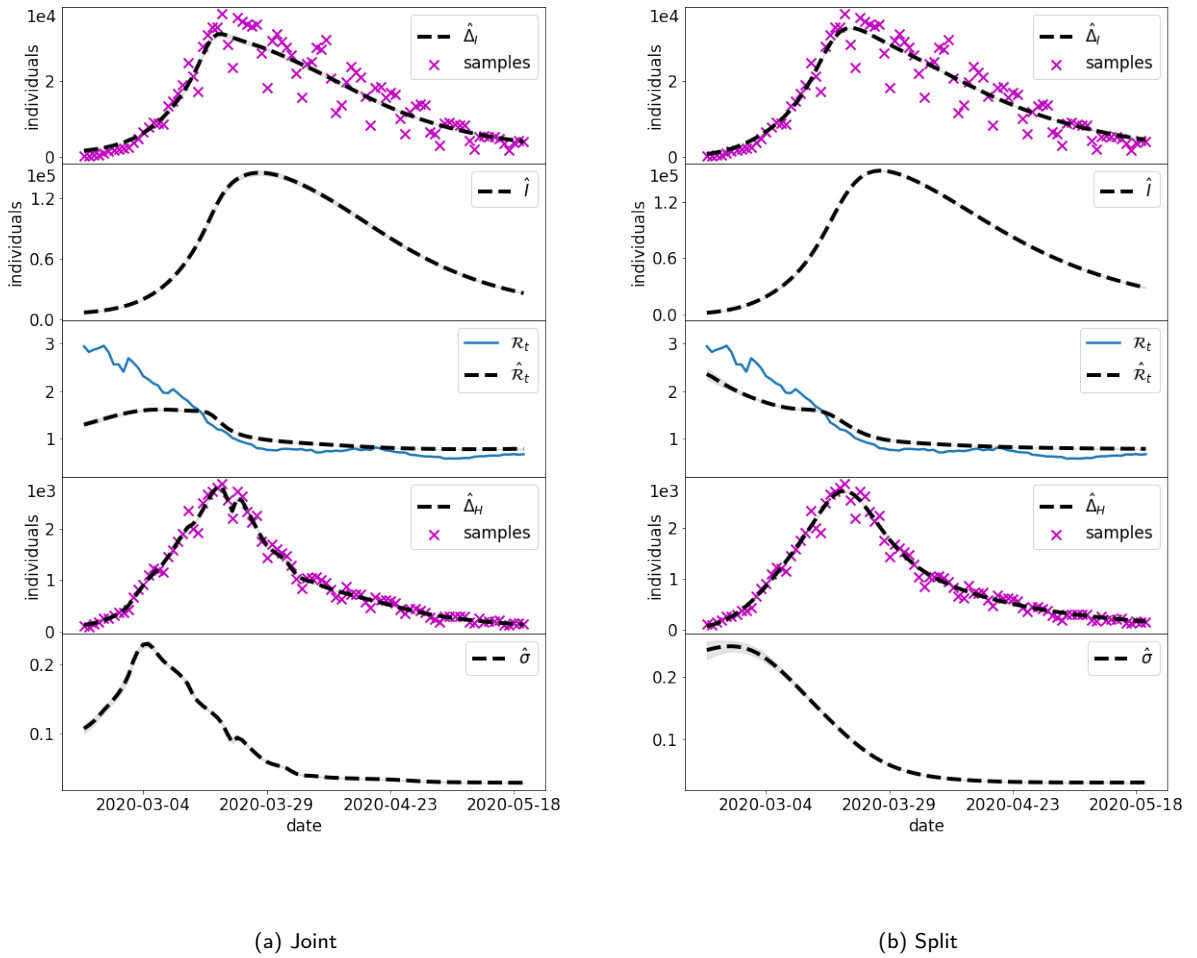


**Figure 10:** Case 7: PINN approximations with the joint (a) and split (b) methods for the real Italian COVID-19 outbreak with  $\sigma$  as a time-dependent parameter. The blue trajectory of  $\mathcal{R}_t$  is the official estimate by ISS.

the joint loss function on data and residual. The second idea consists in implementing a modification to the basic model equations, possibly removing the state variables that are not directly related in the disease transmission and the associated redundant terms in the loss function. This reduced PINN model has been extended to include both infection cases and hospitalization data, which are usually more reliable pieces of information.

Synthetic test Cases 1-3 showed that, when infectious data are subject to small errors, both the split and joint PINN approaches are able to retrieve with high accuracy the system dynamics. The initial training on the data of the split approach provides a clear advantage when minimizing the residual on the model equations and estimating the reproduction number. In fact, it achieves lower errors (up to an order of magnitude) with faster computational times (speed up larger than 60% in Cases 2 and 3). This is probably due to more stable results during the training epochs, as depicted in Figure 2b for a constant transmission (Case 1), and Figure 5 for a time-dependent transmission (Case 2). However, the simultaneous estimate of the initial conditions and the initial transmission proved to be particularly challenging for both PINN approaches (Figures 4 and 6). In fact, even small errors on the data become particularly relevant when there are low number of infections, such as at the beginning of the epidemic. Model results could

improve by assuming a constant initial transmission rate, which is generally in agreement with the free circulation of the pathogen in absence of interventions.

The large errors that typically characterize the data on reported daily infections might deteriorate the retrieval of the temporal changes of the transmission rate and the associated effective reproduction number (Case 4, Figure 7). For this reason, numerous epidemiological analysis are based on data that are not biased by the surveillance system, such as daily hospitalization data, e.g., Bertuzzo et al. (2020). The synthetic test Case 5 shows that the use of daily hospitalizations and infections into the reduced PINN model allowed to improve the accuracy in the estimation of the uncertain time-varying parameters, in particular both the effective reproduction number  $\mathcal{R}_t$  and the fraction of infected individuals requiring hospitalization  $\sigma$ . The split approach still outperforms the joint counterpart with 20% savings in the training cost, however both approaches still present limitations at the beginning of the outbreak.

The application to the Italian COVID-19 epidemic (Cases 6 and 7) emphasizes the importance of considering the fraction of hospitalized individuals,  $\sigma$ , as a temporal-dependent parameter. In fact, the PINN approximations were not able to accurately follow both time series of daily hospitalized and infectious data when considering a constant  $\sigma$  (Figure 9). Results notably improve in the case of a temporal-dependent  $\sigma$  (Figure 10). Many modeling studies assume a constant  $\sigma$ , with possible temporal variations assigned only on the arrival of new disease variants or after the deployment of vaccines. Other processes that might directly impact this parameter are typically neglected. For example, in the early stages of the outbreak, the fear of the new disease might prompt many symptomatic infected individuals to seek health care at the hospital (thus generating a large value of  $\sigma$ ). The subsequent overcrowding of the hospitals and improvement of treatment at home might reduce the value of  $\sigma$  in time. The time-dependent  $\sigma$  values estimated by the PINN approaches (Figure 10) show exactly such a dynamic, with small differences at the beginning. We argue that also in this application the split approach outperforms the joint one. Besides the advantages in the computational times (40% faster), the effective reproduction number obtained with the split approach depicts a closer trajectory to the reference  $\mathcal{R}_t$  estimated by the Italian Institute of Health (Figure 10).

This study focuses on the standard SIR model. While the split approach can be easily adapted to more complex compartmental models (which, for example, consider an exposed compartment, deaths, re-infections, and vaccinations), the reduced equations described in (12) will require ad-hoc formulations depending on the model.

Uncertainty quantification (UQ) is a fundamental ingredient in epidemiological analysis. Unfortunately, it is frequently missing in the PINNs results. Future developments of the proposed split-PINNs approach should consider UQ in more complex compartmental models, for example following the framework proposed by Linka et al. (2022) which combines NNs and Bayesian Inference.

In conclusion, the proposed split PINN-based approach is a robust and easy-to-implement tool to monitor the initial spreading of a disease. It provides estimates of the temporal changes in the model parameters, which is essential to produce more accurate short-term forecasts. Moreover, transfer learning (Bozinovski and Fulgosi, 1976; Xu et al., 2023), i.e. storing knowledge by training a NN on a problem and then applying it to a similar one, can yield cheap and fast generalizations of the model to different outbreaks.

## References

- Berkhahn, S., Ehrhardt, M., 2022. A physics-informed neural network to model COVID-19 infection and hospitalization scenarios. *Advances in Continuous and Discrete Models* 2022, 61. URL: <https://doi.org/10.1186/s13662-022-03733-5>, doi:10.1186/s13662-022-03733-5.
- Bertaglia, G., Lu, C., Pareschi, L., Zhu, X., 2022. Asymptotic-preserving neural networks for multiscale hyperbolic models of epidemic spread. *Mathematical Models and Methods in Applied Sciences* 32, 1949–1985. URL: <https://doi.org/10.1142/2Fs0218202522500452>, doi:10.1142/s0218202522500452.
- Bertuzzo, E., Mari, L., Pasetto, D., Miccoli, S., Casagrandi, R., Gatto, M., Rinaldo, A., 2020. The geography of COVID-19 spread in Italy and implications for the relaxation of confinement measures. *Nature Communications* 11. URL: <https://www.scopus.com/inward/record.uri?eid=2-s2.0-85089903551&doi=10.1038%2fs41467-020-18050-2&partnerID=40&md5=df127b09e09483d96dca80beaf2212e5>, doi:10.1038/s41467-020-18050-2.
- Bozinovski, S., Fulgosi, A., 1976. The influence of pattern similarity and transfer of learning upon training of a base perceptron B2. (original in Croatian: Utjecaj slicnosti likova i transfera učenja na obucavanje baznog perceptrona B2). *Proc. Symp. Informatica* 3, 121–5.
- Cori, A., Ferguson, N.M., Fraser, C., Cauchemez, S., 2013. A New Framework and Software to Estimate Time-Varying Reproduction Numbers During Epidemics. *American Journal of Epidemiology* 178, 1505–1512. URL: <https://doi.org/10.1093/aje/kwt133>, doi:10.1093/aje/kwt133.
- Cybenko, G., 1989. Approximation by superpositions of a sigmoidal function. *Math. Control Signal Systems* 2, 303–314. doi:<https://doi.org/10.1007/BF02551274>.
- Diekmann, O., Heesterbeek, J.A.P., Metz, J.A.J., 1990. On the definition and the computation of the basic reproduction ratio  $R_0$  in models for infectious diseases in heterogeneous populations. *Journal of Mathematical Biology* 28, 365–382. URL: <https://doi.org/10.1007/BF00178324>, doi:10.1007/BF00178324.
- van den Driessche, P., Watmough, J., 2002. Reproduction numbers and sub-threshold endemic equilibria for compartmental models of disease transmission. *Mathematical Biosciences* 180, 29–48. URL: <https://www.sciencedirect.com/science/article/pii/S002556402001086>, doi:10.1016/S0025-5644(02)00108-6.
- EpiCentro, 2020. COVID-19 integrated surveillance: key national data. URL: <https://www.epicentro.iss.it/en/coronavirus/sars-cov-2-integrated-surveillance-data>.
- Feng, L., Chen, Z., Jr, H.A.L., Furati, K., Khaliq, A., Feng, L., Chen, Z., Jr, H.A.L., Furati, K., Khaliq, A., 2022. Data driven time-varying SEIR-LSTM/GRU algorithms to track the spread of COVID-19. *Mathematical Biosciences and Engineering* 19, 8935–8962. URL: <http://www.aimspress.com/article/doi/10.3934/mbe.2022415>, doi:10.3934/mbe.2022415. cc\_license\_type: cc\_by Number: mbe-19-09-415 Primary\_atype: Mathematical Biosciences and Engineering Subject\_term: Research article Subject\_term\_id: Research article.
- Gatto, M., Bertuzzo, E., Mari, L., Miccoli, S., Carraro, L., Casagrandi, R., Rinaldo, A., 2020. Spread and dynamics of the COVID-19 epidemic in Italy: Effects of emergency containment measures. *Proceedings of the National Academy of Sciences* 117, 10484–10491. URL: <https://www.pnas.org/doi/10.1073/pnas.2004978117>, doi:10.1073/pnas.2004978117. publisher: Proceedings of the National Academy of Sciences.
- Glorot, X., Bengio, Y., 2010. Understanding the difficulty of training deep feedforward neural networks, in: Teh, Y.W., Titterton, M. (Eds.), *Proceedings of the Thirteenth International Conference on Artificial Intelligence and Statistics*, PMLR, Chia Laguna Resort, Sardinia, Italy. pp. 249–256. URL: <https://proceedings.mlr.press/v9/glorot10a.html>.
- Gozzi, N., Chinazzi, M., Davis, J.T., Mu, K., Piontti, A.P., Ajelli, M., Perra, N., Vespignani, A., 2022. Anatomy of the first six months of COVID-19 vaccination campaign in Italy. *PLOS Computational Biology* 18, e1010146. URL: <https://journals.plos.org/ploscompbiol/article?id=10.1371/journal.pcbi.1010146>, doi:10.1371/journal.pcbi.1010146. publisher: Public Library of Science.
- Guzzetta, G., Poletti, P., Ajelli, M., Trentini, F., Marziano, V., Cereda, D., Tirani, M., Diurno, G., Bodina, A., Barone, A., Crottogini, L., Gramegna, M., Melegaro, A., Merler, S., 2020. Potential short-term outcome of an uncontrolled COVID-19 epidemic in Lombardy, Italy, February to March 2020. *Eurosurveillance* 25, 2000293. URL: <https://www.eurosurveillance.org/content/10.2807/1560-7917.ES.2020.25.12.2000293>, doi:10.2807/1560-7917.ES.2020.25.12.2000293. publisher: European Centre for Disease Prevention and Control.
- Haghighat, E., Juanes, R., 2021. SciANN: A Keras/TensorFlow wrapper for scientific computations and physics-informed deep learning using artificial neural networks. *Computer Methods in Applied Mechanics and Engineering* 373, 113552. URL: <https://www.sciencedirect.com/science/article/pii/S0045782520307374>, doi:<https://doi.org/10.1016/j.cma.2020.113552>.
- Hornik, K., Stinchcombe, M., White, H., 1989. Multilayer feedforward networks are universal approximators. *Neural Networks* 2, 359–366. URL: <https://www.sciencedirect.com/science/article/pii/0893608089900208>, doi:[https://doi.org/10.1016/0893-6080\(89\)90020-8](https://doi.org/10.1016/0893-6080(89)90020-8).
- Ionides, E.L., Nguyen, D., Atchadé, Y., Stoev, S., King, A.A., 2015. Inference for dynamic and latent variable models via iterated, perturbed Bayes maps. *Proceedings of the National Academy of Sciences* 112, 719–724. URL: <https://www.pnas.org/doi/10.1073/pnas.1410597112>, doi:10.1073/pnas.1410597112. publisher: Proceedings of the National Academy of Sciences.
- ISTAT, 2020. Primi risultati dell'indagine di sieroprevalenza sul SARS-CoV-2. Technical Report. Istituto Nazionale di Statistica, Ministero della Salute (Italia). URL: <https://www.istat.it/it/files//2020/08/ReportPrimiRisultatiIndagineSiero.pdf>.
- Kingma, D.P., Ba, J., 2017. Adam: A Method for Stochastic Optimization arXiv:1412.6980.
- Lemaitre, J., Pasetto, D., Zanon, M., Bertuzzo, E., Mari, L., Miccoli, S., Casagrandi, R., Gatto, M., Rinaldo, A., 2022. Optimal control of the spatial allocation of COVID-19 vaccines: Italy as a case study. *PLoS Computational Biology* 18. URL: <https://www.scopus.com/inward/record.uri?eid=2-s2.0-85134430806&doi=10.1371%2fjournal.pcbi.1010237&partnerID=40&md5=a1f1b300642e5d4c9f8592566f36b173>, doi:10.1371/journal.pcbi.1010237.
- Linka, K., Schäfer, A., Meng, X., Zou, Z., Karniadakis, G.E., Kuhl, E., 2022. Bayesian Physics Informed Neural Networks for real-world nonlinear dynamical systems. *Computer Methods in Applied Mechanics and Engineering* 402, 115346. URL: <https://www.sciencedirect.com/science/article/pii/S0045782522004327>, doi:10.1016/j.cma.2022.115346.

- Long, J., Khaliq, A.Q.M., Furati, K.M., 2021. Identification and prediction of time-varying parameters of COVID-19 model: a data-driven deep learning approach. *International Journal of Computer Mathematics* 98, 1617–1632. URL: <https://doi.org/10.1080/00207160.2021.1929942>. publisher: Taylor & Francis \_eprint: <https://doi.org/10.1080/00207160.2021.1929942>.
- Malinzi, J., Gwebu, S., Motsa, S., 2022. Determining COVID-19 Dynamics Using Physics Informed Neural Networks. *Axioms* 11, 121. URL: <https://www.mdpi.com/2075-1680/11/3/121>, doi:10.3390/axioms11030121. number: 3 Publisher: Multidisciplinary Digital Publishing Institute.
- Mari, L., Casagrandi, R., Bertuzzo, E., Pasetto, D., Miccoli, S., Rinaldo, A., Gatto, M., 2021. The epidemicity index of recurrent SARS-CoV-2 infections. *Nature Communications* 12. URL: <https://www.scopus.com/inward/record.uri?eid=2-s2.0-85105782342&doi=10.1038%2fs41467-021-22878-7&partnerID=40&md5=81043db0cce92e38d048797358fc7ab1>, doi:10.1038/s41467-021-22878-7.
- Marziano, V., Guzzetta, G., Mammone, A., Riccardo, F., Poletti, P., Trentini, F., Manica, M., Siddu, A., Bella, A., Stefanelli, P., Pezzotti, P., Ajelli, M., Brusaferrero, S., Rezza, G., Merler, S., 2021a. The effect of COVID-19 vaccination in Italy and perspectives for living with the virus. *Nature Communications* 12, 7272. doi:10.1038/s41467-021-27532-w.
- Marziano, V., Guzzetta, G., Rondinone, B.M., Bocconi, F., Riccardo, F., Bella, A., Poletti, P., Trentini, F., Pezzotti, P., Brusaferrero, S., Rezza, G., Iavicoli, S., Ajelli, M., Merler, S., 2021b. Retrospective analysis of the Italian exit strategy from COVID-19 lockdown. *Proceedings of the National Academy of Sciences* 118, e2019617118. URL: <https://www.pnas.org/doi/10.1073/pnas.2019617118>, doi:10.1073/pnas.2019617118. publisher: Proceedings of the National Academy of Sciences.
- Ning, X., Guan, J., Li, X.A., Wei, Y., Chen, F., 2023. Physics-Informed Neural Networks Integrating Compartmental Model for Analyzing COVID-19 Transmission Dynamics. *Viruses* 15, 1749. URL: <https://www.mdpi.com/1999-4915/15/8/1749>, doi:10.3390/v15081749. number: 8 Publisher: Multidisciplinary Digital Publishing Institute.
- Olumoyin, K.D., Khaliq, A.Q.M., Furati, K.M., 2021. Data-Driven Deep-Learning Algorithm for Asymptomatic COVID-19 Model with Varying Mitigation Measures and Transmission Rate. *Epidemiologia* 2, 471–489. URL: <https://www.mdpi.com/2673-3986/2/4/33>, doi:10.3390/epidemiologia2040033. number: 4 Publisher: Multidisciplinary Digital Publishing Institute.
- Parolini, N., Dede', L., Ardenghi, G., Quarteroni, A., 2022. Modelling the COVID-19 epidemic and the vaccination campaign in Italy by the SUIHTER model. *Infectious Disease Modelling* 7, 45–63. URL: <https://www.sciencedirect.com/science/article/pii/S2468042722000100>, doi:10.1016/j.idm.2022.03.002.
- Pasetto, D., Finger, F., Rinaldo, A., Bertuzzo, E., 2017. Real-time projections of cholera outbreaks through data assimilation and rain-fall forecasting. *Advances in Water Resources* 108, 345–356. URL: <https://www.scopus.com/inward/record.uri?eid=2-s2.0-85006056338&doi=10.1016%2fj.advwatres.2016.10.004&partnerID=40&md5=99267a7112d02ae159fd60526e5081c9>, doi:10.1016/j.advwatres.2016.10.004.
- Pasetto, D., Lemaitre, J., Bertuzzo, E., Gatto, M., Rinaldo, A., 2021. Range of reproduction number estimates for COVID-19 spread. *Biochemical and Biophysical Research Communications* 538, 253–258. URL: <https://www.scopus.com/inward/record.uri?eid=2-s2.0-85097883800&doi=10.1016%2fj.bbrc.2020.12.003&partnerID=40&md5=d068f09e9f822c846763ab52953bf6f6>, doi:10.1016/j.bbrc.2020.12.003.
- Raissi, M., Perdikaris, P., Karniadakis, G.E., 2017a. Physics Informed Deep Learning (Part I): Data-driven Solutions of Nonlinear Partial Differential Equations *arXiv:1711.10561*.
- Raissi, M., Perdikaris, P., Karniadakis, G.E., 2017b. Physics Informed Deep Learning (Part II): Data-driven Discovery of Nonlinear Partial Differential Equations *arXiv:1711.10566*.
- Raissi, M., Perdikaris, P., Karniadakis, G.E., 2019. Physics-informed neural networks: A deep learning framework for solving forward and inverse problems involving nonlinear partial differential equations. *Journal of Computational Physics* 378, 686–707.
- Schiassi, E., De Florio, M., D'Ambrosio, A., Mortari, D., Furfaro, R., 2021. Physics-Informed Neural Networks and Functional Interpolation for Data-Driven Parameters Discovery of Epidemiological Compartmental Models. *Mathematics* 9, 2069. URL: <https://www.mdpi.com/2227-7390/9/17/2069>, doi:10.3390/math9172069.
- Torku, T.K., Khaliq, A.Q.M., Furati, K.M., 2021. Deep-Data-Driven Neural Networks for COVID-19 Vaccine Efficacy. *Epidemiologia* 2, 564–586. URL: <https://www.mdpi.com/2673-3986/2/4/39>, doi:10.3390/epidemiologia2040039. number: 4 Publisher: Multidisciplinary Digital Publishing Institute.
- Trevisin, C., Bertuzzo, E., Pasetto, D., Mari, L., Miccoli, S., Casagrandi, R., Gatto, M., Rinaldo, A., 2023. Spatially explicit effective reproduction numbers from incidence and mobility data. *Proceedings of the National Academy of Sciences of the United States of America* 120, e2219816120. doi:10.1073/pnas.2219816120.
- Wang, S., Yu, X., Perdikaris, P., 2021. When and why PINNs fail to train: A neural tangent kernel perspective. *Journal of Computational Physics* , 110768 URL: <https://www.sciencedirect.com/science/article/pii/S002199912100663X>, doi:<https://doi.org/10.1016/j.jcp.2021.110768>.
- Xu, C., Cao, B.T., Yuan, Y., Meschke, G., 2023. Transfer learning based physics-informed neural networks for solving inverse problems in engineering structures under different loading scenarios. *Computer Methods in Applied Mechanics and Engineering* 405, 115852. URL: <https://www.sciencedirect.com/science/article/pii/S0045782522008088>, doi:<https://doi.org/10.1016/j.cma.2022.115852>.
- Ziarelli, G., Dede', L., Parolini, N., Verani, M., Quarteroni, A., 2023. Optimized numerical solutions of SIRDVW multiage model controlling SARS-CoV-2 vaccine roll out: An application to the Italian scenario. *Infectious Disease Modelling* 8, 672–703. URL: <https://www.ncbi.nlm.nih.gov/pmc/articles/PMC10240908/>, doi:10.1016/j.idm.2023.05.012.